NASA TECHNICAL MEMORANDUM

NASA TM X-71734

NASA TM X-71734

HOT CORROSION EVALUATION OF ALUMINIDE COATED SUPERALLOYS IN SUPPORT OF AN ASTM ROUND ROBIN PROGRAM

by Gilbert Santoro
Lewis Research Center
Cleveland, Ohio 44135

July, 1975

HOT CORROSION EVALUATION OF ALUMINIDE COATED SUPERALLOYS IN SUPPORT OF AN ASTM ROUND ROBIN PROGRAM

by Gilbert Santoro

Lewis Research Center

SUMMARY

The current lack of a standardized evaluation test for the hot corrosion resistance of coated alloys has prompted ASTM Committee C-22.6 to initiate a round robin program. While participating in this program LeRC conducted an investigation not only to fulfill the round robin requirements to evaluate coated superalloys under controlled test conditions but to provide a description of the corrosion process by which the coatings failed.

Two commercial aluminized coatings on three substrates (IN-713C, IN-100 and B-1900) were hot corroded at 900°C in a 0.3 mach burner rig with 5ppm synthetic sea salt and at two cycling frequencies. Extensive post-exposure examinations were conducted on the corroded specimens such as metallography, x-ray diffraction, scanning electron microscopy, microprobe raster scans, and spectrographic analyses. Thermodynamic calculations were made of the equilibrium burner flame composition and the calculations were compared to the experimental findings.

It was found that localized spalling of the coatings preceded coating failure. It was suggested that the spalling of the coatings was due to the formation of

localized stresses caused by the depletion of chromium and aluminum in the coating or the enrichment of the coating with sulfur. For the materials and test conditions investigated, it was found that coating life was dependent only upon the initial coating thickness and not on the type of aluminized coating, the substrate, or the cycle frequency.

INTRODUCTION

As new coatings for gas turbine blades and vanes are developed to resist hot corrosion attack they are commonly evaluated in burner rig tests to establish their protection ability (ref. 1). Currently there is no standard evaluation test. Thus, it is difficult to compare or to use the test data from different laboratories. For this reason ASTM Committee G-22.6 initiated a round robin program on the hot corrosion of coated superalloys with LeRC as one of the participants. LeRC had previously participated in the round robin on the hot corrosion of uncoated superalloys in which 15 laboratories exposed identical materials using similar test conditions (ref. 2). A comparison of the results revealed that the participants were in fair agreement as to those alloys with the most and with the least corrosion resistance but they were unable to draw a finer comparison.

In the present program the participants were required to expose, at 900°C, two commerical aluminide coatings applied to IN-713C, IN-100 and B-1900. Exposure was to be in the combustion gases of a burner rig containing synthetic

sea salt. The initial thicknesses of the coatings were to be measured and the time to coating failure recorded. Duplicate runs were to be made using ten minute cycles.

At LeRC this program was extended beyond that required by the ASTM Committee in an attempt to identify the corrosion process. The additional effort towards this end consisted of another set of burner rig exposures at a different cycle frequency and of extensive post-exposure examinations of the specimens, using metallography, x-ray diffraction (XRD), scanning electron microscope (SEM), electron microprobe raster scans and spectrographic analyses. Also thermodynamic calculations were made of the equilibrium burner flame composition at the various temperatures, including 900°C.

This paper presents the combined results of LeRC's contribution to the round robin on the hot corrosion of coated alloys and a description of the corrosion process by which these coatings failed.

EXPERIMENTAL PROCEDURES

Specimens

The substrate alloys used in this study were IN-713C, IN-100 and B-1900. Each substrate was coated with two different aluminide coatings identified by the ASTM Committee only as coating A and coating B.

In all, there were six substrate-coating combinations, three substrates each with two different coatings. Test specimens of these six combinations and the uncoated alloys were cyclindrically shaped, about 1.3cm (0.5 inches) in diameter by about 7.6cm (3 inches) long.

In order to conserve specimens, the as-received evaluations were made after the burner rig exposures on the base of the specimens (that length within the holder). These evaluations consisted of determining the initial coating thickness, XRD, and metallography. The initial coating thickness was measured on metallographically prepared cross-sections with a microscopic cathetometer at a magnification of 100X. The coating thickness is defined in this program as that distance from the surface of the specimen to the visually unaffected substrate. Thus, coating thickness includes the diffusion zone beneath the coating proper. The measured values are listed in Table I along with the values from the vendor. Except for coating A on IN-713C, the agreement with the unidentified vendor's values are considered good. The predominate phase detected in the coating by XRD was

βNiAl (beta nickel aluminide). In most cases weak lines of alpha alumina, αAl_2O_3, were also observed, see Table II. Figure 1, (a) through (f), shows the microstructure of the as-received coatings and their substrates. Both coatings have complex microstructures with the structure of the diffusion zone dependent upon the substrate. With the B-coatings even the structure of the coating proper seems somewhat dependent on the substrate. Elemental analysis by the scanning electron microscope's energy dispersive x-ray spectrum shows that the dark particles in coating A to be predominately (aluminum) Al, probably αAl_2O_3, in correlation with the XRD results. In both coatings (A and B) the elemental distribution is qualitatively the same. As an example of this distribution the details for coating A on IN-713C will be given. In the coating proper, figure 2(a), the intensity of the (nickel), Ni, peak predominates. The (chromium), Cr, and the Al peaks are about the same height, about 1/5th that of the Ni peak. There is also a slight indication of a (titanium), Ti, peak. The Cr intensity increases slightly near the diffusion zone, figure 2(b). In the diffusion zone just below the coating proper the Ni and Cr peaks have about the same height, figure 2(c). There are also a small (molybdenum), Mo, peak a slight Al peak and an indication of a Ti peak. In the diffusion zone near the substrate, figure 2(d), the Ni peak again predominates, the Cr peak has decreased and the Mo and Al peaks have remained about the same. There is here a measurable Ti peak. In the substrate near its interface with the diffusion zone, the relative peak heights

are Ni>>Cr>>Mo > Al > Ti, figure 2(e).

Burner Rig Procedures

A listing of the burner rig parameters and the specimen's temperature profile are given in Table III. The rig was operated at a velocity of 0.3 mach and used type A-1 fuel (ASTM D-1655) with a sulfur content of 0.02 to 0.05 weight percent. Synthetic sea salt (ASTM D-1141) was added to the combustion chamber at a concentration of 5ppm. The rig accommodated up to eight specimens. Each specimen extended 5.08cm (2 inches) above the specimen holder. The temperatures were measured optically and corrected using the value from a calibration run in which a thermocouple was embedded within the center of a similarly shaped dummy specimen, 2.54cm (one inch) from its top (the middle of the hot zone). Three sets of tests were conducted: (1) Duplicate runs of coated alloys cycling 10 minutes at temperature and three minutes of forced air cooling; (2) Singular runs of uncoated alloys using the same cycle as in (1); and (3) Singular run of coated alloys cycling one hour at temperature and three minutes of forced air cooling. The first two sets were Round Robin requirements while the latter was extra inorder to determine if cycle frequency affected spalling.

During all runs the specimens were periodically inspected and weighed. Initially this was done after each 20 cycles. But because of the short lives of the coatings, the interval was shortened to every five cycles. The

inspection consisted of a binocular examination at a magnification of 10X for the purpose of determining coating failure. Coating failure was defined by the ASTM Round Robin directive as the appearance of a random pit with a diameter 1270 microns (50 mils) or greater which penetrated to the substrate. Complete penetration was discernible by the presence of green oxide in the pit. The color of the oxides from the coatings ranged from brownish to blue-green and were readily distinguishable from the green-yellowish oxides growing within the pits (or on the uncoated substrates). The uncoated alloys were arbitrarly exposed for 40 hours.

The post burner rig evaluations of the specimens were mostly made in the area of the hot zone and consisted of XRD, spectrographic analyses, metallography, SEM, and EMP raster scans.

Thermodynamic calculations were made using the data and the NASA computer program described in ref. 3. This computer program is based on the minimization of free energy approach to chemical equilibrium calculations subject to the constraints of maintaining a proper mass balance between reactants and products. The program can handle simultaneously up to fifteen separate reactants composed of up to fifteen chemical elements and calculates the composition of product mixtures composed of up to 150 separate condensed or gaseous species.

RESULTS

Weight change results are given in figure 3, (a) through (f), for the 10 minute cycle runs and in figure 4, (a) through (c), for the one hour cycle runs. The data points where coating failures were first observed are marked with "F". Most often coating failure was preceded by a decrease in the slope of the weight change curve, indicating the on-set of spalling. It was observed that the spalling was not restricted to the oxide scale. The coating also spalled. Usually the coating began to spall shortly before coating failure, i.e., the time when the slope of the weight change curves decreased. For example, with coating B on IN-100 no spalling of the coating was observed up to 30 hours at temperature, figure 5(a). After 30 hours the slope of the weight change curve decreased, figure 3(d). After 45 hours the coating failed. A pit was observed in one of the areas vacated by the spalled coating, figure 5(b). Failure pits were often found in areas where the coating had spalled. A magnified view of a pit in such an area is shown in figure 5(c). Thus spalling of the coating is a factor in coating failure.

Coating failure times are presented in Table IV. The data are for 10 minute cycle runs (duplicates) and for one hour cycle runs. When the data are specified as time to failure per unit initial coating thickness it is seen that specific time to failure is related essentially to initial coating thickness and is apparently not dependent on cycle frequency, substrate composition, or type of coating (A or

B). Coating failure occurred randomly along the exposed length of the specimen, i.e., sometimes in the hot zone (zone of maximum temperature) and other times above or below the hot zone. Most often more than one failure pit was observed in the same specimen. In most of the coated specimens failure occurred on that surface of the pin facing away from the flame (the backside). It is probable the backside temperature is higher than the flame side temperature. The circular arrangement of the specimens in their holder may prevent the heat from radiating as readily from the backside area as from the flame side. Of the uncoated alloys, IN-713C was the most corrosion resistant and IN-100 the least resistant, figure 5. But, as was noted above, the substrate chemistry apparently does not affect coating life.

Table II lists the post exposure XRD results. The predominate oxide along the entire length of all the pins was αAl_2O_3. Various crystalline forms of sodium sulfate were observed but for simplicity they were all listed in the Table as (sodium-sulfate), Na_2SO_4. Figure 7, (a) through (f), shows photomicrographs of the cross-sections from the hot zones of the corroded coated specimens after their coating had failed. Much of the oxide scale has spalled off and that which remains is porous and therefore probably non-protective. Beneath the oxide scale most of the coating still persists but it has undergone a discernable change in its morphology. In the area of a pit, figure 8, the coating is completely consumed and much of the oxide scale has spalled. The retained scale is complex, porous and contains

long diagonal cracks. The energy dispersive x-ray spectrum provision of the SEM and raster scans from the electron probe reveal a depletion of the Al and Cr concentration in what is left of the coating after corrosion. This depletion was observed in the coating proper and in the diffusion zone and accounts for the change in the morphology of the coating noted above. The distribution of the elements in the substrate just below the diffusion zone was not altered. A comparison of figure 9 with figure 2(c) provides an example of the depletion within the diffusion zone, particularly of the Cr. The distribution of sulfur in the corroded specimens is also of interest. This element was detected in the scale near the scale-coating interface and throughout the coating proper but not in the diffusion zone. It was found by raster scan to exist in clumps rather than being uniformally distributed. Figure 10 is an example of the sulfur distribution.

Results of the thermodynamic calculations are presented in Table V. The imput to the computer program based on the burner rig parmeters used in this Round Robin program are listed in Table V(A). Selected products of the computer readout are given in Table V(B). Product concentrations are listed for two temperatures, 1660°C (the flame temperature) and 900°C (the maximum metal temperature). The condensed phases at 900°C were found to be Na_2SO_4, MgO, (magnesia) and CaO (calcia). The molar ratios of their cations were calculated and compared to the concentration of these elements found by spectrographic analyses of the salt condensed on the coated specimens. This comparison is

listed in Table V(C) and is qualitatively in agreement, i.e., the amount of (sodium), Na, > (magnesium), Mg > (calcium), Ca. Quantitative agreement ought not to be expected as the analyzed deposits condensed at various temperatures due to the temperature gradient along the specimen as listed in Table III. Further the computer readout shows that Na_2SO_4 condensation is very temperature sensitive. A 30° C temperature variation from 900°C will cause about a 45 % change in the mole fraction concentration of deposited Na_2SO_4.

DISCUSSION

A number of explanations to account for hot corrosion have been published (ref. 4-9). An excellent review of the entire field is given in ref.10. It is generally agreed that the culprit in hot corrosion in gas turbine engines is Na_2SO_4, formed when ingested salt in the air reacts with the sulfur in the fuel,

$$2NaCl(g) + H_2O(g) + SO_3(g) = Na_2SO_4(g) + 2HCl(g)$$

But a necessary condition for hot corrosion to occur is that the Na_2SO_4 condenses,

$$Na_2SO_4(g) = Na_2SO_4(c)$$

From Table V(B) it is seen that Na_2SO_4 ought to be produced in the burner flame and that it ought to condense on the entire exposed surface of the specimens under the conditions of this test. The experimental results confirm these expectations. Along the entire exposed surface of the specimen the presence of sodium sulfate was detected by XRD

and the cations of the predicted condensed salts were detected by spectrographic analyses. Thus failure pits were found in the hot zone as well as outside the hot zone.

It has been observed that αAl_2O_3 scales are prone to spall in cyclic tests, both in pure oxidation and in hot corrosion (ref. 11). The scales of the coated alloys in this program do spall. But the scales are porous and probably non-protective. So scale spalling is probably not a significant factor in the corrosion process. More important is the fact that the coatings spalled. The spallation of aluminized coatings has been observed before (ref. 12). The spalling was attributed to the susceptibility of the brittle coatings (β NiAl) to thermal shock. To overcome this the aluminum content of the coatings was decreased (to 22-24 weight percent) in that study in the hope of lowering the ductile-to-brittle transition temperature. Coating life was increased but the coatings continued to spall. In the present program the spalling of the coatings occurred randomly at small local areas and sometimes extended to the substrate thereby directly causing a failure pit. Most often the spall did not extend to the substrate but it did provide a shorter path for corrosion to the substrate thus creating a favorable site for the formation of a failure pit. It is also important to note that most of the coating did not spall. Rather it corroded along a more or less uniform front. The localized nature of the spallation of the coatings suggests the presence of local stresses in the coatings. These stresses need not have been present when

the coatings were fabricated but could have developed during corrosion as the result of the depletion of elements in the coatings such as the Al and the Cr or the enrichment of the coatings with sulfur. This suggestion is consistent with the observation that the coatings did not begin to spall until well into the test, i.e., shortly before failure when the slope of their weight change curve began to decrease. If thermal shock had primarily caused the spalling, then the coatings should have begun to spall immediately. Further, any shock induced cracks would provide new surfaces for corrosion resulting in corrosion fingers penetrating through the coating. But no cracks in the coating or corrosion penetrations were observed (see figure 7). The development of localized stresses is also consistent with the noted insensitivity of failure times to changes in cycle frequency. During the interval required for the development of stresses, differences in cycle frequency ought not affect the process which at this stage is essentially a diffusion process. Once the stresses have developed to the point of exceeding coating strength, the coating begins to spall and failure occurs shortly afterwards. The short interval between the time the coating begins to spall and coating failure mirimizes any influence cycle frequency would have during this stage of the process. It can be assumed that the mechanism for failure is similar for both coatings as they are both aluminide coatings with about the same composition. This assumption implies that the Al_2O_3 particles in the A coatings had no effect on the corrosion process. Since the substrate compositions have remained

essentially the same during the corrosion process, neither contributing nor depleting elements from the coatings, the substrates should not play a major role in the coatings' failure.

Thus localized spalling of the coatings and the formation of failure pits is the process by which the coatings fail. The exact cause of the spalling of the coatings is not known. Since most of the coating corrodes along a more or less uniform front it can be assumed the spalling of the coatings is due to the development of localized stresses which may be related to the depletion of elements from the coatings or the enrichment of the coatings by sulfur. Whatever the cause, coating life in this study was dependent only upon the initial coating thickness and not on the type of coating (A or B), the substrate , or the cycle frequency.

CONCLUSIONS

The conclusions based upon the results obtained in this investigation of the hot corrosion of three aluminide-coated nickel base superalloys are as follows:

1) For the materials and test conditions investigated, time to coating failure is primarily dependent upon initial coating thickness and not upon coating type, substrate composition or cycle frequency.

2) Coating failure is due to localized spalling of the coating which leads directly to a failure pit or creates a favorable site for the subsequent formation of a failure pit.

REFERENCES

1. Hot Corrosion Problems Associated with Gas Turbines. STP-421, Am. Soc. Testing Mater., 1966.
2. Hot Corrosion in Gas Turbines: Mechanisms, Alloy and Coating Development, Environmental Effects, and Evaluation. NMAB-260, National Materials Advisory Board (AD-870745), 1970.
3. Kohl, F. J.; Stearns, C. A.; and Fryburg, G. C.: Sodium-Sulfate: Vaporization Thermodynamics and Role in Corrosive Flames. Presented at the Intern. Symp. on Metal-Slag-Gas Reactions and Processes sponsored by Electrochemical Society, May 11-16, 1975, Toronto, Canada.
4. Simons, E. L.; Browning, G. V.; and Liebhafsky, H. A.: Sodium Sulfate in Gas Turbines Corrosion, vol. 11, No. 12, 1955, pp. 17-25.
5. Seybolt, A. U.: Contribution to the Study of Hot Corrosion. AIME Trans., vol. 242, No. 9, Sept. 1968, pp. 1955-1961.
6. Bornstein, N. S.; and DeCrescente, M. A.: The Relationship Between Compounds of Sodium and Sulfur and Sulfidation. AIME Trans., vol. 245, No. 9, Sept. 1969, pp. 1947-1952.
7. Goebel, J. A.; and Pettit, F. S.: Na_2SO_4-Induced Accelerated Oxidation (Hot Corrosion) of Nickel. Met. Trans., vol. 1, No. 7, July 1970, pp. 1943-1954.

8. Goebel, J. A.; and Pettit, F. S.: The Influence of Sulfides on the Oxidation Behavior of Nickel-Base Alloys. Met. Trans., vol. 1, No. 12, Dec. 1970, pp. 3421-3429.

9. Gobel, J. A.; Pettit, F. S.; and Goward, G. W.: Hot Corrosion Mechanism in Stationary Gas Turbines. Deposition and Corrosion in Gas Turbines, Anthony B. Hart and A. J. B. Cutler, eds., John Wiley and Sons, 1973, pp. 96-114.

10. Stringer, J.: Hot Corrosion in Gas Turbines. MCIC-72-08, Battelle Columbus Labs. (AD-745474), 1972.

11. Giggin, C. S.; and Pettit, F. S.: Oxide Scale Adherence Mechanisms. PWA-5042, Pratt & Whitney Aircraft Co., 1974.

12. Moore, Victor S.; and Stetson, A. R.: Hot Corrosion Resistant Aluminide Coatings of Controlled Composition for Nickel Base Superalloys. RDR-1702-3, International Harvester Co. (AD-767728), 1973.

TABLE I. - AS-RECEIVED THICKNESS OF THE COATINGS

Substrate Alloy	Coating Thickness						Cycle Interval (minutes)
	Vendor's Values (microns)		This Program's Values* (microns)				
			Coating A		Coating B		
	Coating A	Coating B	0°	90°	0°	90°	
IN-713C	51-58	91	91	84	79	76	10
			94	91	86	94	10
			91	91	89	89	60
IN-100	76-84	74	71	71	66	66	10
			78	76	58	71	10
			91	89	71	78	60
B-1900	76-99	61	91	81	61	66	10
			76	89	56	56	10
			91	99	48	51	60

* Measurements made on the base of the specimen upon completion of burner rig exposure. Measurements made at two orientations 90° apart.

TABLE II. - X-RAY DIFFRACTION OF HOT CORRODED COATED ALLOYS

Substrate	Coating	Distance From Top of Specimen (cm)	Phases (listed in order of decreasing line intensities)
IN-713C	A	0.64 (1/4")	αAl_2O_3
		2.54 (1")*	αAl_2O_3, Na_2SO_4, β(NiAl), $\gamma'(Ni_3Al)$
		4.44 (1 3/4")	αAl_2O_3, Na_2SO_4, NiO(?)
		Base	β(NiAl), αAl_2O_3
IN-713C	B	0.64 (1/4")	αAl_2O_3, $\gamma'(Ni_3Al)$, β(NiAl)
		2.54 (1")*	αAl_2O_3
		4.44 (1 3/4")	αAl_2O_3, Na_2SO_4, $\gamma'(Ni_3Al)$
		Base	β(NiAl), αAl_2O_3
IN-100	A	0.64 (1/4")	αAl_2O_3, Na_2SO_4
		2.54 (1")*	αAl_2O_3, Na_2SO_4, $\gamma'(Ni_3Al)$
		4.44 (1 3/4")	αAl_2O_3, β(NiAl)
		Base	β(NiAl), $\gamma'(Ni_3Al)$
IN-100	B	0.64 (1/4")	αAl_2O_3, $\gamma'(Ni_3Al)$, Na_2SO_4
		2.54 (1")*	αAl_2O_3
		4.44 (1 3/4")	αAl_2O_3, Na_2SO_4, $\gamma'(Ni_3Al)$
		Base	β(NiAl), αAl_2O_3
B-1900	A	0.64 (1/4")	αAl_2O_3, Na_2SO_4, $\gamma'(Ni_3Al)$
		2.54 (1")*	αAl_2O_3, $\gamma'(Ni_3Al)$
		4.44 (1 3/4")	αAl_2O_3, $\gamma'(Ni_3Al)$, β(NiAl), Na_2SO_4
		Base	β(NiAl), αAl_2O_3
B-1900	B	0.64 (1/4")	αAl_2O_3, β(NiAl), $\gamma'(Ni_3Al)$
		2.54 (1")*	αAl_2O_3, β(NiAl), $\gamma'(Ni_3Al)$
		4.44 (1 3/4")	αAl_2O_3, β(NiAl), $\gamma'(Ni_3Al)$, Na_2SO_4
		Base	β(NiAl), $\gamma'(Ni_3Al)$

* middle of the hot zone

TABLE III. - BURNER RIG TEST PARAMETERS

RIG: 0.3 mach Pratt-Whitney type.

FUEL: Type A-1, ASTM D-1655. Dissolved sulfur content over one year period varied from 0.02 to 0.05 weight percent.

AIR/FUEL RATIO: Approximately 25/1 at one atmosphere pressure.

SALT: 5ppm synthetic sea salt, ASTM D-1141.

TEMPERATURE: Maximum metal temperature, 900°C. Temperature profile given below.

CYCLE: Ten minutes and one hour exposures at peak metal temperature with three minutes cooling in forced air at 3.4×10^4 N/m^2 (5psi).

Temperature Profile

Distance from top of specimen (cm)	(inches)	Temperature (°C)
0.64	0.25	860
1.27	0.5	882
1.91	0.75	896
2.54	1.0	896
3.18	1.25	885
3.81	1.5	870
4.45	1.75	837

TABLE IV. - FAILURE TIMES OF COATED ALLOYS

Specimen	Time to Failure hours (cycles)			Specific Time to Failure* hours per micron		
	Ten Minute Cycles (duplicate runs)		One Hour Cycles	Ten Minute Cycles (duplicate runs)		One Hour Cycles
IN-713C						
Coating A	60 (360)	70 (420)	60 (60)	0.7	0.8	0.6
Coating B	45 (270)	55 (330)	70 (70)	0.5	0.7	0.8
IN-100						
Coating A	40 (240)	40 (240)	30 (30)	0.5	0.6	0.3
Coating B	40 (240)	45 (270)	55 (55)	0.6	0.7	0.7
B-1900						
Coating A	55 (330)	55 (330)	55 (55)	0.6	0.7	0.6
Coating B	40 (240)	40 (240)	45 (45)	0.6	0.7	0.9

*Time to failure divided by the initial coating thickness.

TABLE V. - THERMODYNAMIC ANALYSIS VIA COMPUTER PROGRAM*

(A) PROGRAM INPUT:

Fuel composition (ASTM D-1655):	$CH_{1.9185}$, $\Delta H_{298°K}$ = -5300 cal/moles	
Sulfur content of fuel	:	0.05 weight percent
Fuel inlet temperature	:	298°K
Composition of air	:	N(1.56176), O(0.41959), Ar(0.009324), C(0.000300), $\Delta H_{298°K}$ = -28.2 cal/mole
Moisture in the air	:	one weight percent (approximately 50% relative humidity at 298°K)
Salt concentration	:	5ppm
Salt composition**	:	

salt	weight percent
NaCl	68.78
$MgCl_2$	14.57
Na_2SO_4	11.46
$CaCl_2$	3.25
KCl	1.93

Pressure	:	one atmosphere
Inlet temperature	:	298°K
Air to fuel ratio	:	25/1

* Program and data from ref. (4).
** The five most abundant inorganic salts which make up the ASTM standard substitute ocean water (ASTM D-1141).

(B) PRODUCT CONCENTRATIONS

Species	Concentration (mole fraction)	
	1660°C*	900°C*
Na_2SO_4 (gas)	1.900×10^{-15}	4.650×10^{-8}
Na_2SO_4 (liquid)	0	5.5207×10^{-7}
CaO (gas)	6.549×10^{-11}	1.473×10^{-22}
CaO (solid)	0	4.0288×10^{-8}
MgO (gas)	9.734×10^{-9}	7.204×10^{-18}
MgO (solid)	0	2.0997×10^{-7}
NaCl (gas)	5.7198×10^{-8}	5.7687×10^{-7}
SO_2 (gas)	2.1448×10^{-5}	1.9481×10^{-5}
SO_3 (gas)	3.260×10^{-8}	1.4197×10^{-6}
HCl (gas)	1.9305×10^{-6}	1.5390×10^{-6}
H_2O (gas)	1.0886×10^{-1}	1.0953×10^{-1}

* 900°C is the maximum specimen temperature and 1660°C is the burner flame temperature.

(C) COMPARISION WITH SPECTROGRAPHIC ANALYSIS

Molar Ratio	
Spectrographic analysis (Na / Mg / Ca)	computer output (Na / Mg / Ca)
9.4/ 2/1	15.1/5.2/1

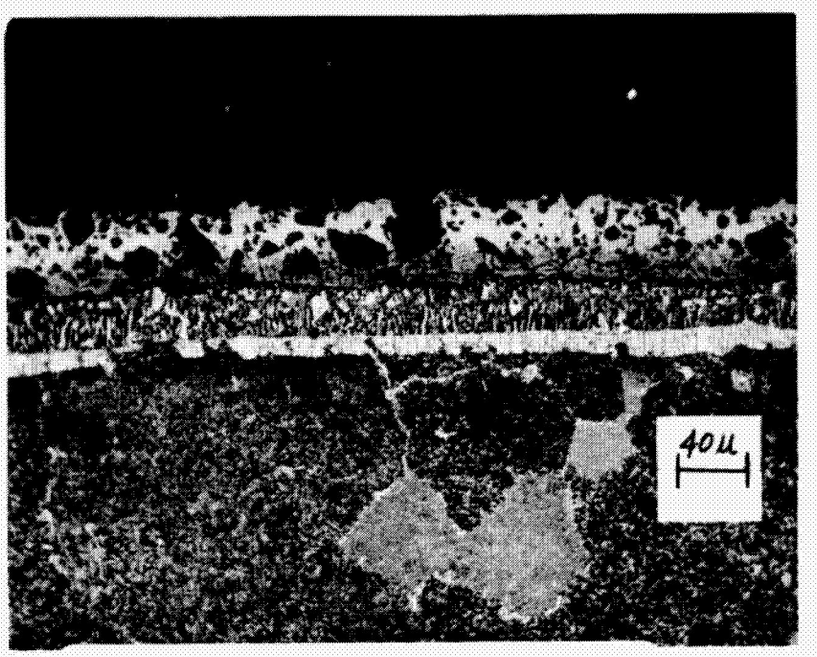

(a) IN-713C Coating A

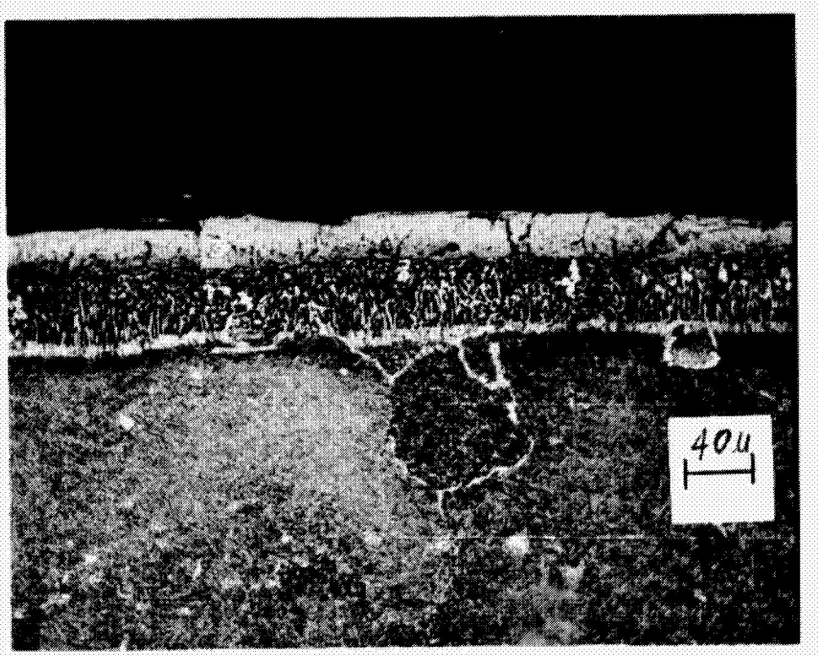

(b) IN-713C Coating B

Figure 1. - Microstructure of the as-received coatings showing the coating proper, the diffusion zone and the substrate.

(c) IN-100 Coating A

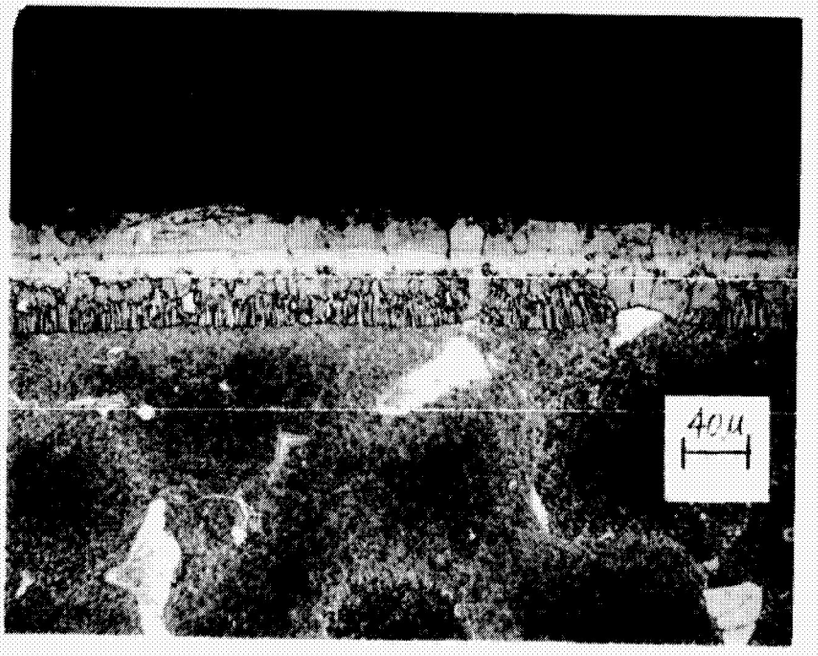

(d) IN-100 Coating B

Figure 1. - continued

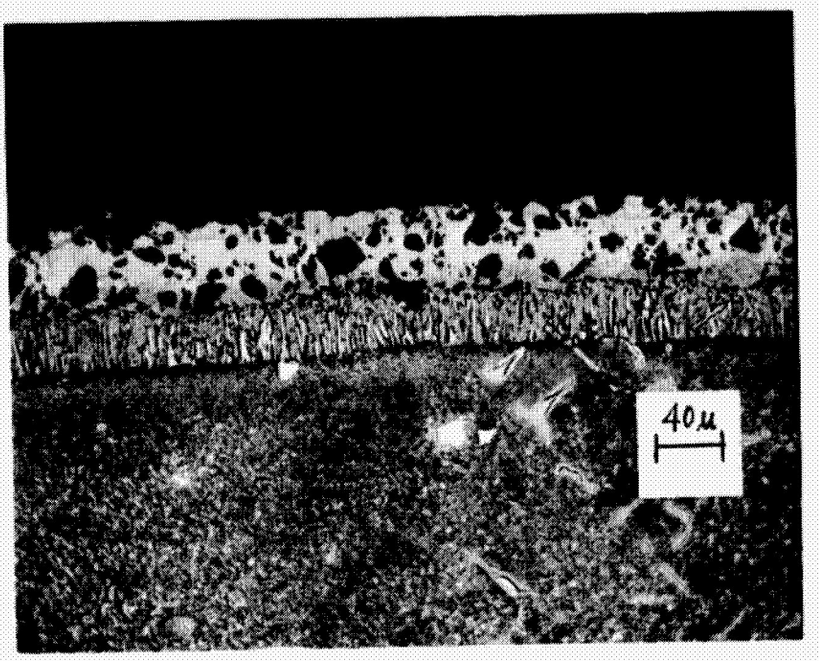

(e) B-1900 Coating A

(f) B-1900 Coating B

Figure 1. - continued

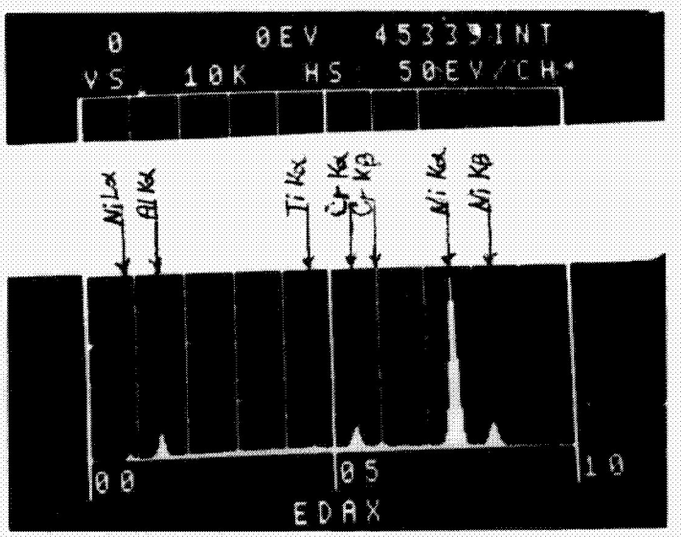

(a) Analysis of elements midway within the coating proper.

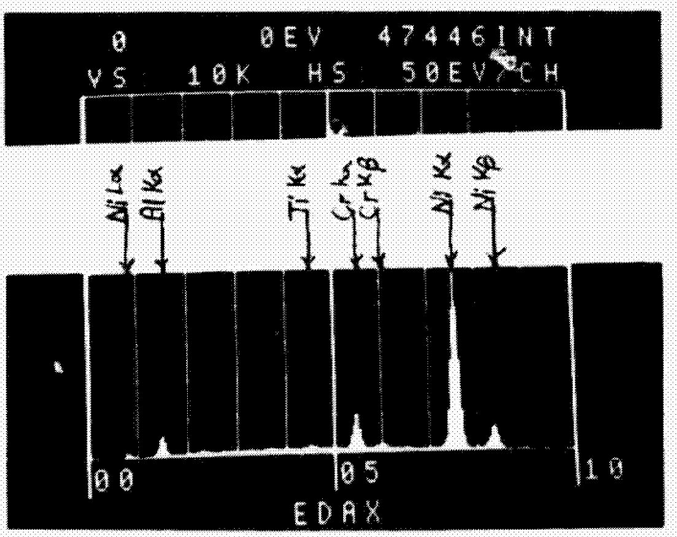

(b) Analysis of elements in the coating proper near the diffusion layer.

Figure 2. - Energy dispersive spectrum for elements in coating A on IN-713C, as-received.

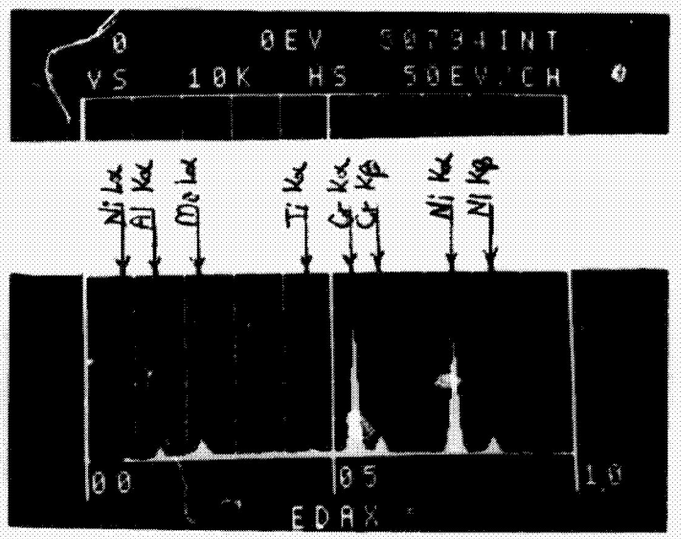

(c) Analysis of elements in the diffusion layer near the coating proper.

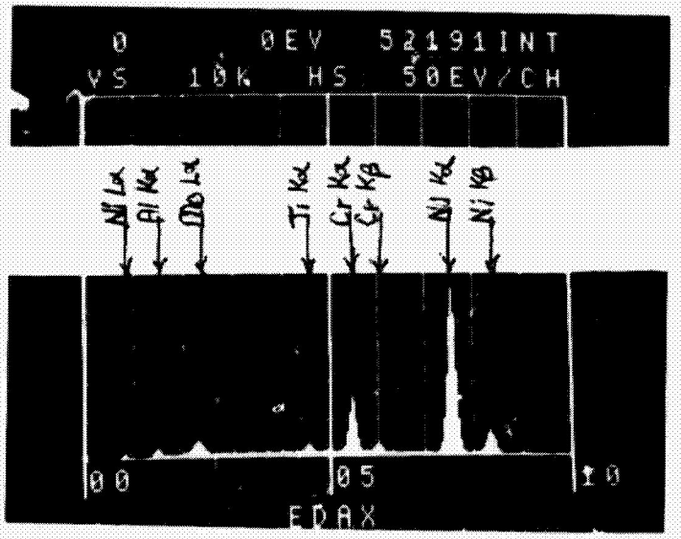

(d) Analysis of elements in the diffusion layer near the substrate.

Figure 2. - continued

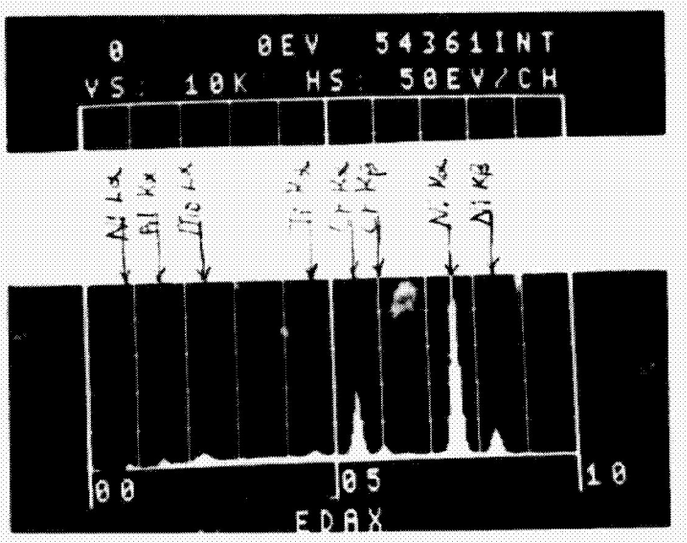

(e) Analysis of elements in the substrate alloy near the coating.

Figure 2. - concluded

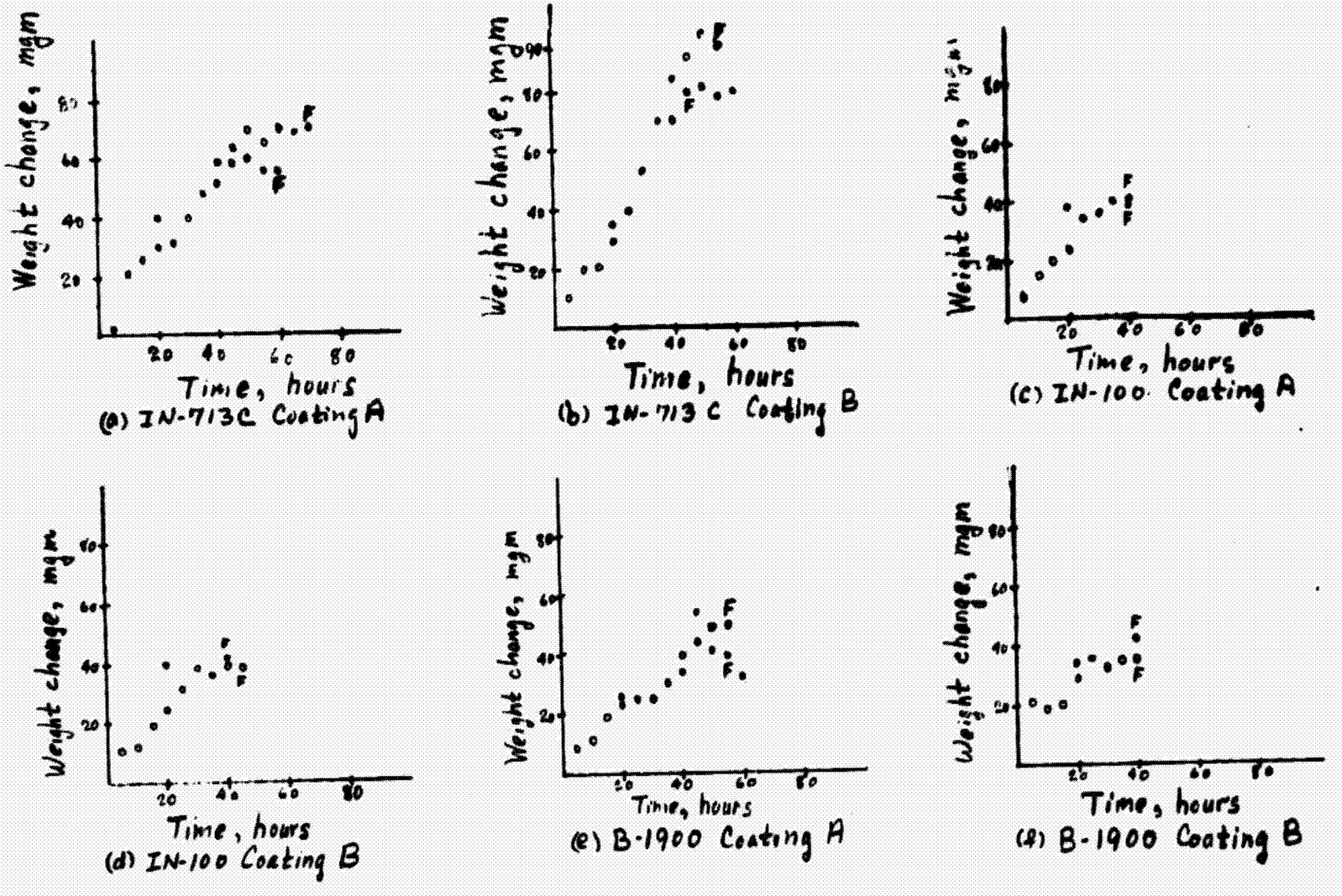

Figure 3. - Weight change of coated alloys at 900°C and ten minutes cycles. Failure occurred at points marked "F".

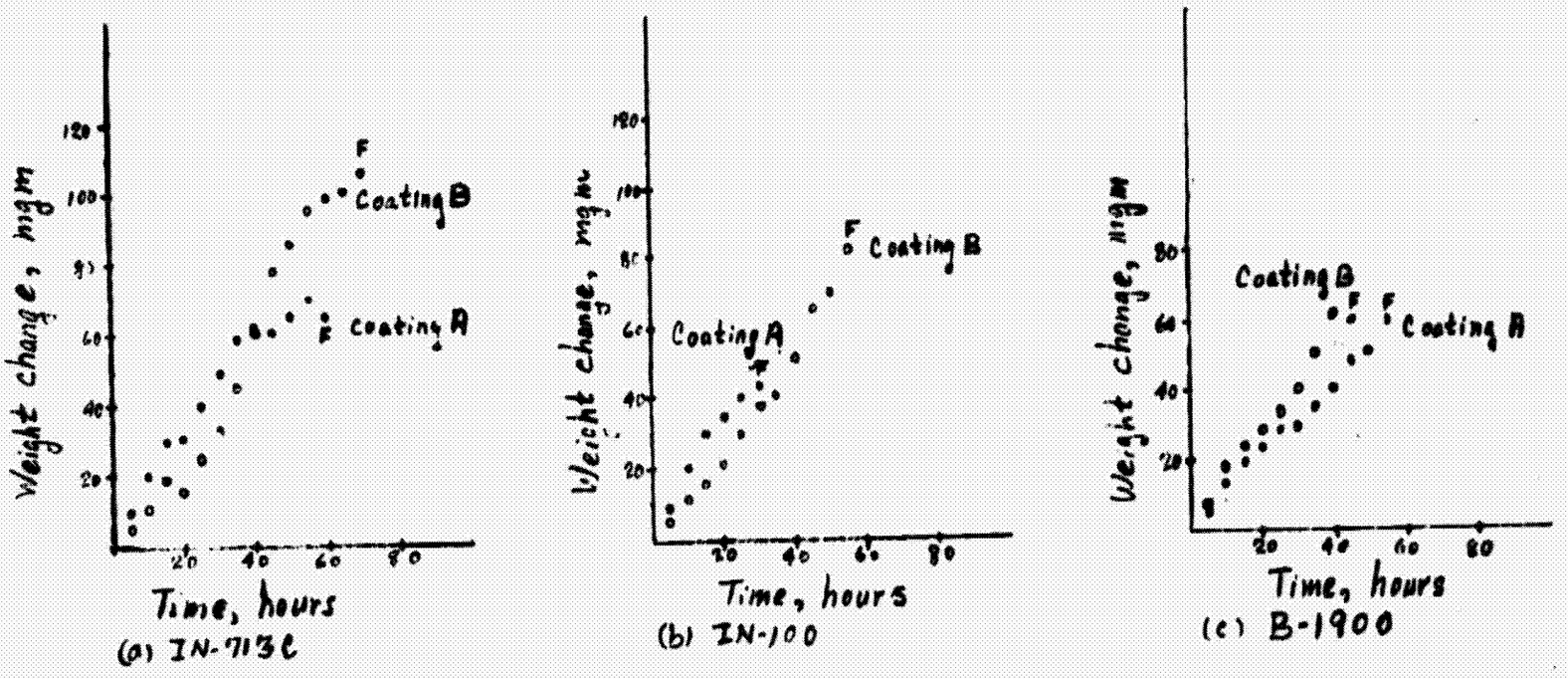

Figure 4. - Weight change of coated alloys at 900°C and one hour cycles. Failure occurred at points marked "F".

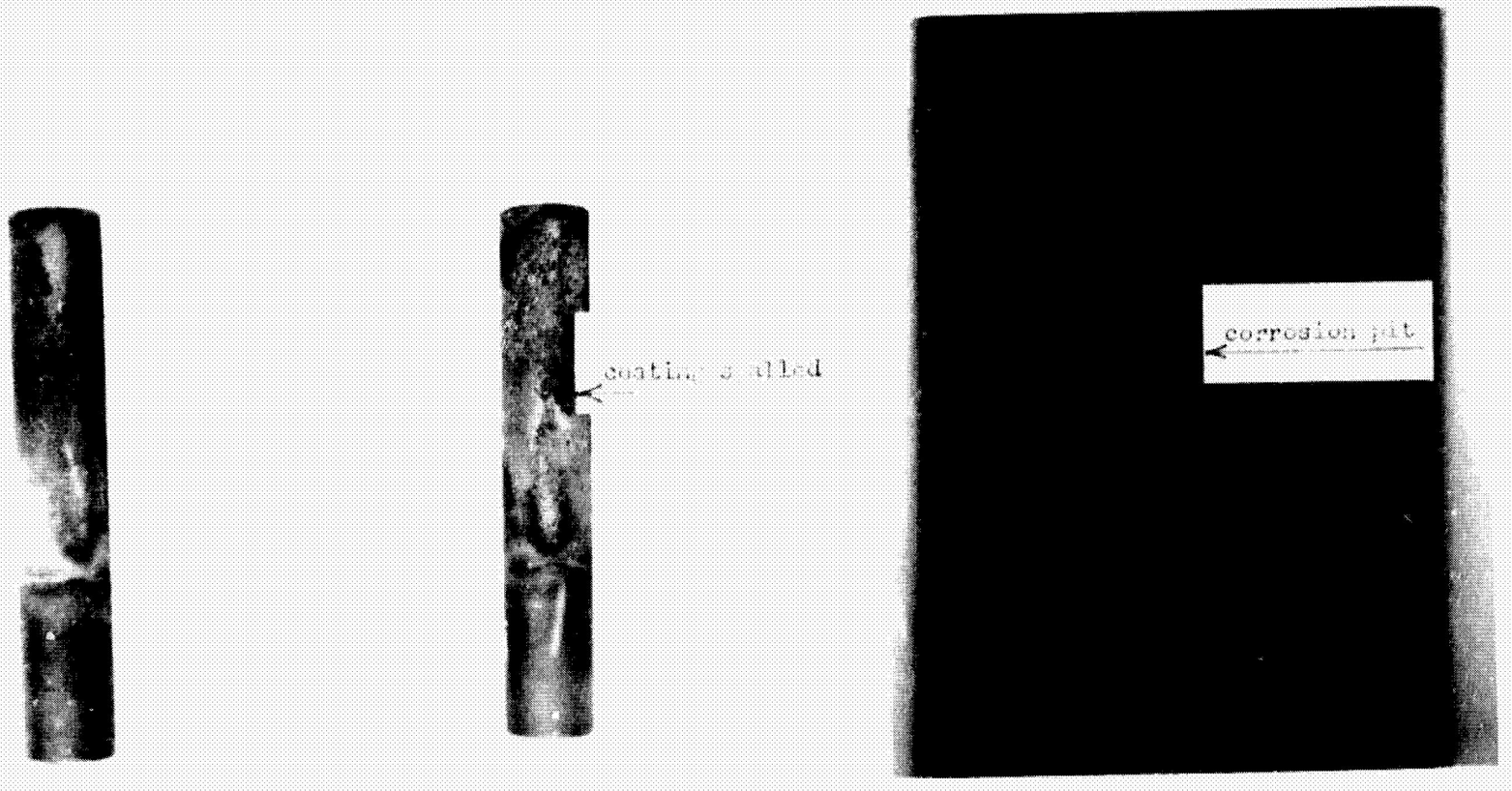

(a) IN-100 Coating B corroded 30 hours, 10 minutes cycles. Coating has not spalled.

(b) IN-100 Coating B corroded 45 hours, 10 minutes cycles. Coating has spalled.

(c) IN-713C Coating B. Area of spalled coating with corrosion pit. Magnified about 10X.

Figure 5. - Spallation of the coating and the development of corrosion pits.

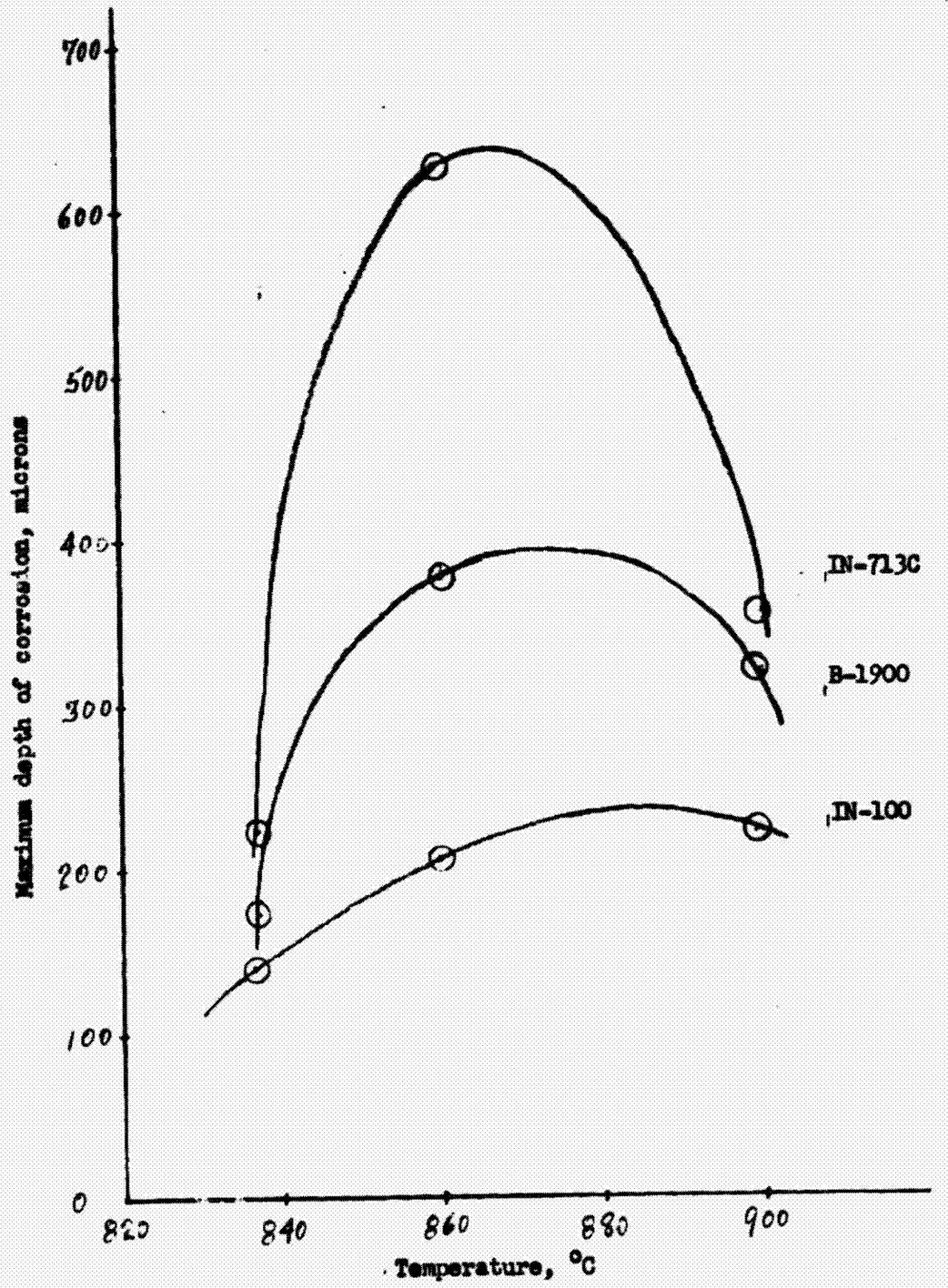

Figure 6. - Corrosion of uncoated alloys in the 0.3 mach burner rig after 40 hours exposure to 5ppm synthetic sea salt and with 10 minute cycles.

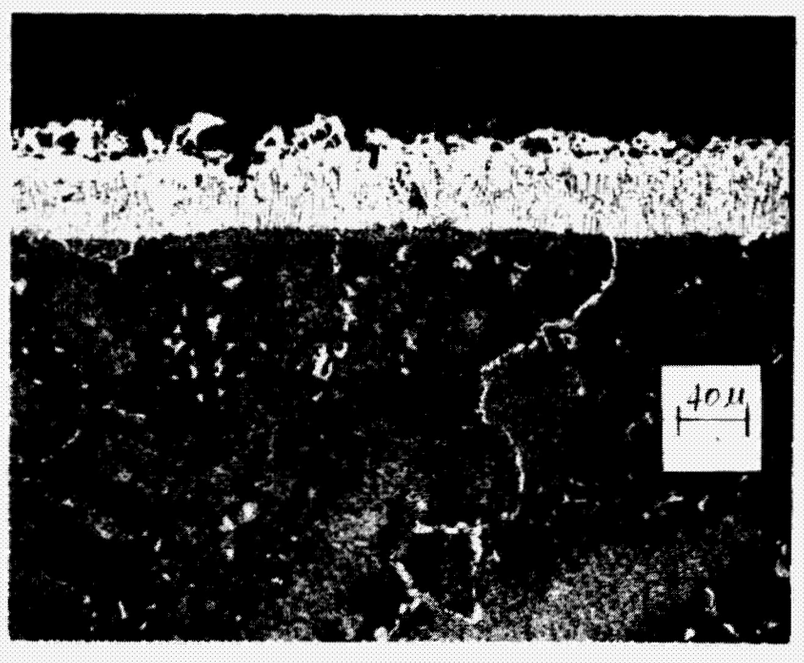

(a) IN-713C Coating A hot zone. Corroded 900°C, 70 hours, 10 minute cycles.

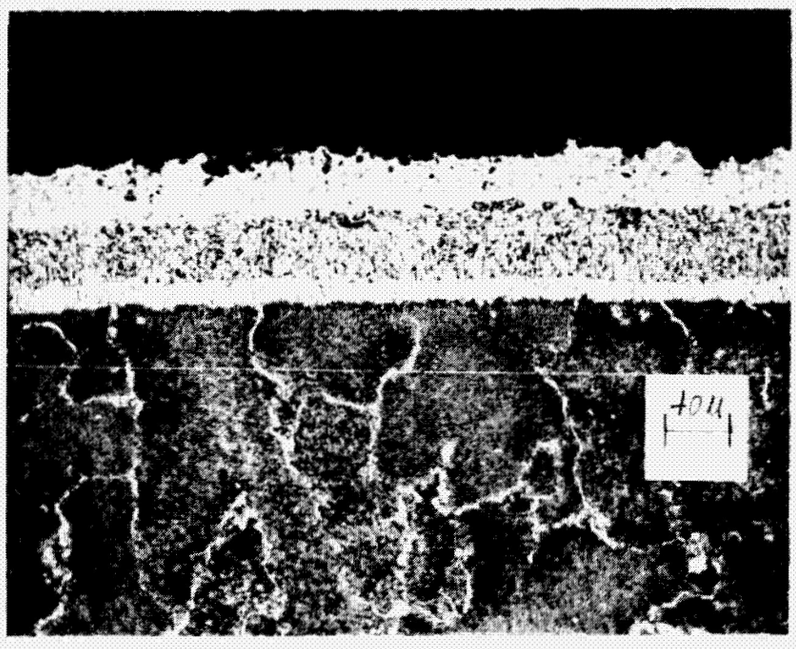

(b) IN-713C Coating B hot zone. Corroded 900°C, 55 hours, 10 minute cycles.

Figure 7. - Microstructure of the corroded coatings showing the oxide scale, coating proper, diffusion layer, and the substrate.

(c) IN-100 Coating A hot zone. Corroded 900°C, 40 hours, 10 minute cycles.

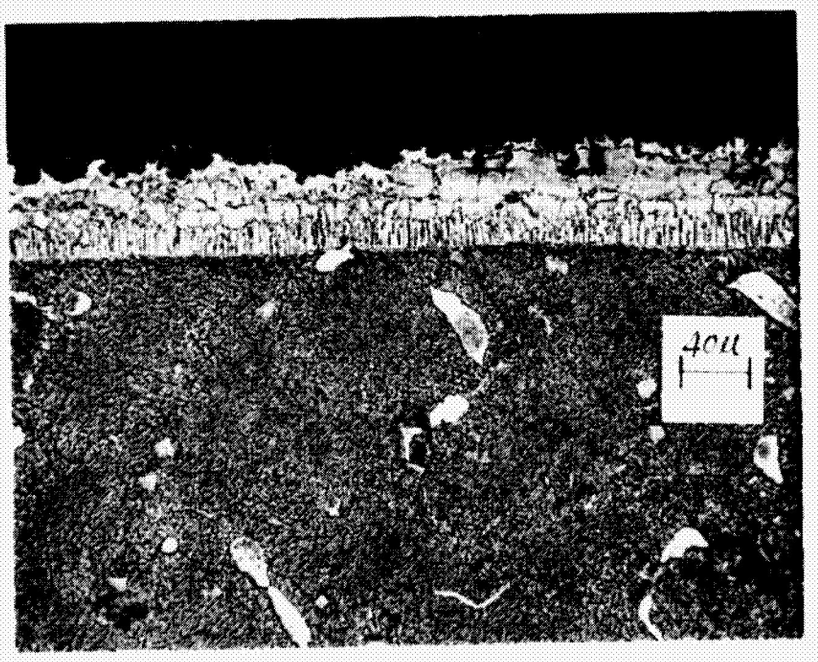

(d) IN-100 Coating B hot zone. Corroded 900°C, 45 hours, 10 minute cycles.

Figure 7. - continued

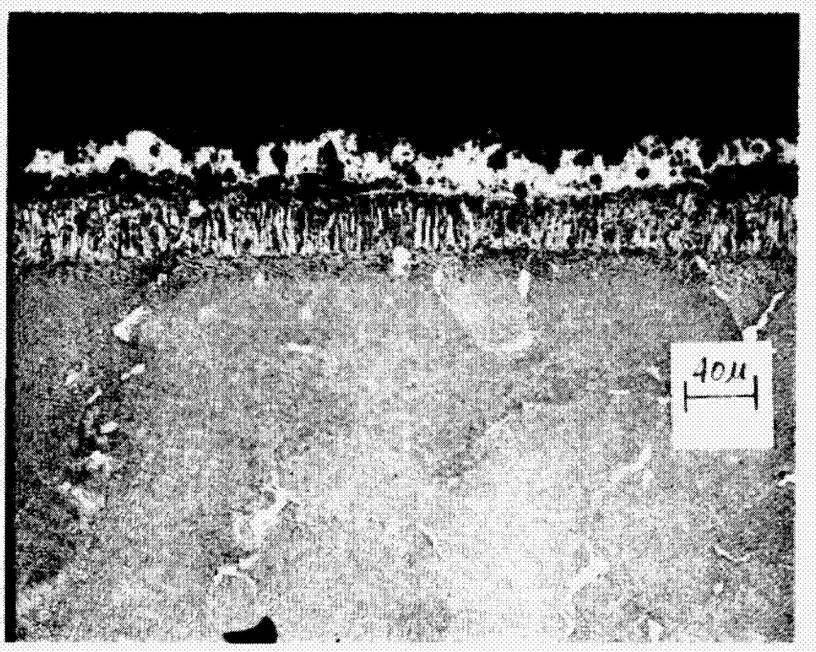

(e) B-1900 Coating A hot zone. Corroded 900°C, 55 hours, 10 minute cycles.

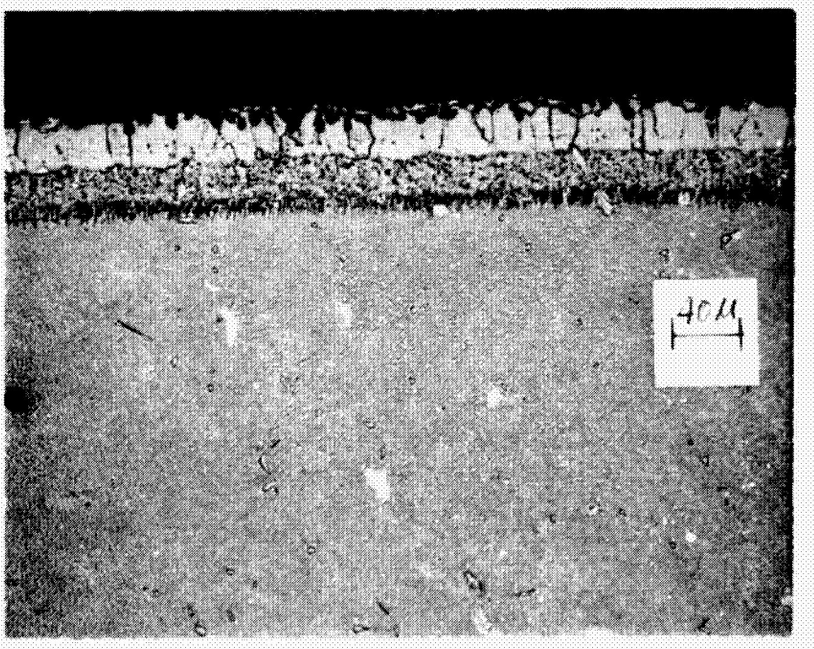

(f) B-1900 Coating B hot zone. Corroded 900°C, 40 hours, 10 minute cycles.

Figure 7. - concluded

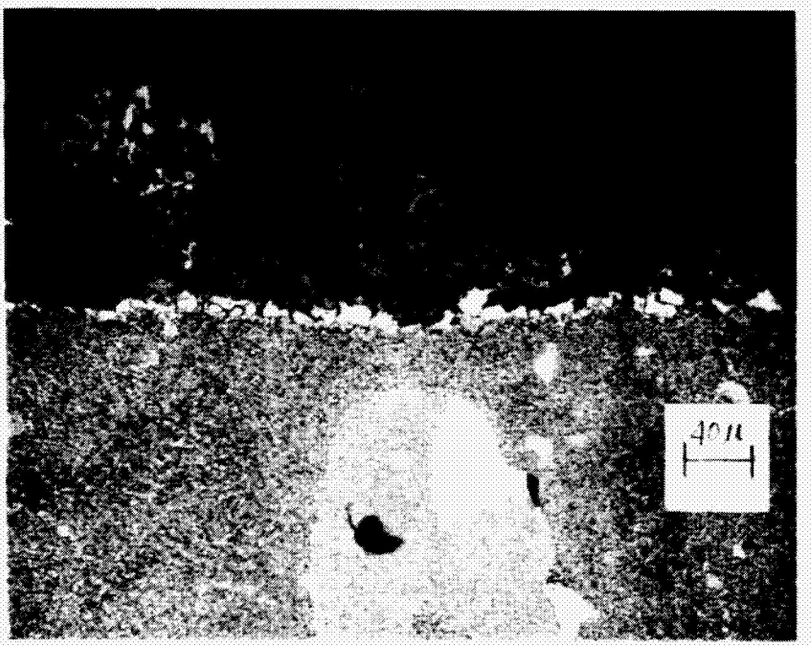

Figure 8. - Microstructure of a corrosion pit in IN-100 coating A.

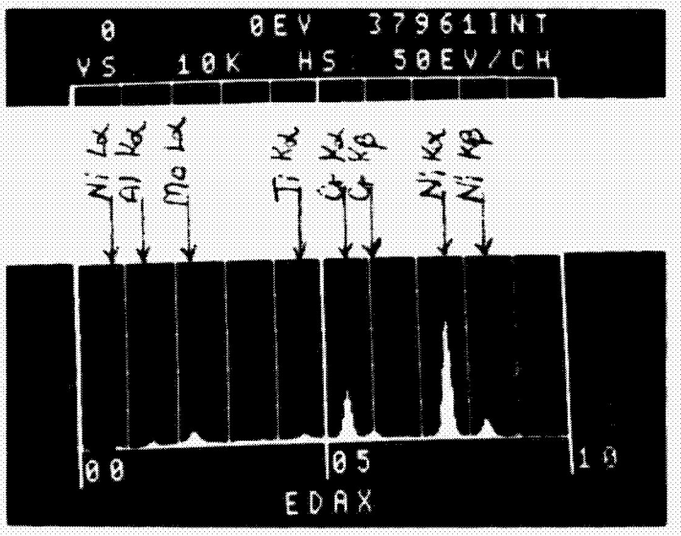

Figure 9.- Energy dispersive x-ray spectrum for elements in the diffusion layer of coating A on IN-713C, corroded at 900°C, ten minute cycles.

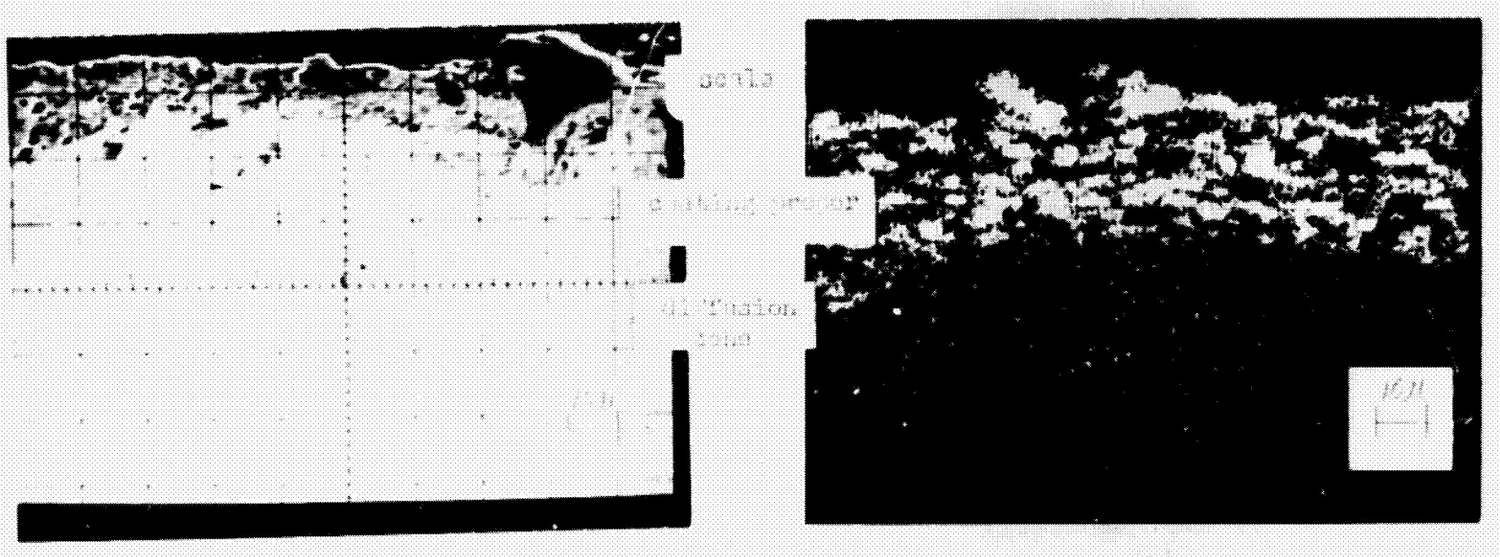

(a) Electron micrograph of IN-713C Coating A. Corroded 300°C, 10 minute cycles.

(b) Raster scan of $S_{K\alpha}$ on area shown in (a), somewhat shifted to the left.

Figure 10. - Sulfur distribution in Coating A on IN-713C showing the sulfur distributed in clumps in the scale and the coating proper but not in the coating's diffusion zone.